Journal of Power Sources 196 (2011) 4646–4654

Contents lists available at ScienceDirect

Journal of Power Sources

journal homepage: www.elsevier.com/locate/jpowsour

Effect of gas diffusion layer modulus and land–groove geometry on membrane stresses in proton exchange membrane fuel cells

Zongwen Lu[a], Changsik Kim[b], Anette M. Karlsson[a], James C. Cross III[b], Michael H. Santare[a,*]

[a] Department of Mechanical Engineering, University of Delaware, Newark, DE 19716, USA
[b] Nuvera Fuel Cells Inc., Billerica, MA 01821, USA

ARTICLE INFO

Article history:
Received 15 November 2010
Received in revised form 7 January 2011
Accepted 10 January 2011
Available online 19 January 2011

Keywords:
Fuel cell
Proton exchange membrane
Gas diffusion layer
Geometry
In-plane stresses
Compression test

ABSTRACT

The electrical functionality of PEM fuel cells is facilitated by minimizing the contact resistances between different materials in the fuel cell, which is achieved via compressive clamping. The effect of the gas diffusion layer (GDL) modulus on the in-plane stress in the membrane after clamping is studied via numerical simulations, including both isotropic and anisotropic GDL properties. Furthermore, the effect of cell width and land–groove width ratio on the in-plane stress in the membrane subjected to a single hygro-thermal cycle is investigated for aligned and alternating gas channel geometries. The results from varying the GDL properties suggest that the in-plane stress in the membrane after clamping is due to a non-linear and coupled interaction of GDL and membrane deformation. The results of the geometric studies indicate that when the gas channels are aligned, the cell width and land–groove width ratio affect the in-plane stress distribution, but do not significantly affect the stress magnitudes. However, when the gas channels are alternating, the cell width and land–groove width ratio have significant effect on the membrane in-plane stresses. The effect of land–groove geometry is qualitatively verified by a series of experimental compression tests.

1. Introduction

Durability of proton exchange membranes (PEMs) during long-term operation is a major obstacle to widespread commercialization of proton exchange membrane fuel cells (PEMFCs). The PEMs are prone to failure in the form of chemical degradation and mechanical damage [1–6]. Studies have shown that the mechanical stresses, due to hygro-thermal cycles in the membrane, are primarily responsible for the mechanical damage [7–11]. Therefore, investigating the stresses in the membrane during hygro-thermal cycling is an important step toward understanding the failure mechanisms in the membrane.

Previous simulation work in our lab showed that the in-plane stress is the dominant stress in PEM membranes during hygro-thermal loading [10]. Furthermore, compressive, plastic deformation may occur during the hygro-thermal loading, resulting in tensile residual stresses after unloading, which may explain the occurrence of cracks and pinholes in the membrane under cyclic loading [8]. In addition, the membrane stresses strongly depend on the swelling anisotropy [12]. As an extension of our previous work, this work investigates (i) the effect of the gas diffusion layer (GDL) modulus, and (ii) land–groove geometry on the in-plane stress in the membrane.

A typical GDL is a carbon fiber material (either woven or non-woven), is generally between 100 and 300 μm thick, and used on both the PEMFC anode and cathode side. The GDL is the most deformable component in a PEM fuel cell stack [13]. Some researchers have studied the effect of the GDL on fuel cell performance [14–17], and it is well recognized that the GDL can greatly influence PEM fuel cell performance. However, little work has been published on the effect of GDL properties on the membrane stresses. Thus, we perform a parametric, two-dimensional, numerical study to investigate the effect of GDL modulus on the membrane in-plane stresses after clamping.

PEM fuel cells today are engineered largely according to one of two major flow field architectures: (1) directed flows in independent, segregated channels or grooves, separated by lands (e.g., a corrugated plate), or (2) open flows through a macroporous structure (e.g., a mesh or foam). In either case, the flow field structure simultaneously provides mechanical support and electrical connectivity. In the present study, we contrast these two paradigms by both the length scales and densities of the features providing the support of the membrane electrode assembly (MEA). Several publications exploring the effect of fuel cell geometry on fuel cell performance can be found in the literature [18–21], and these studies agree that the fuel cell performance depends on the geometry.

* Corresponding author. Tel.: +1 302 831 2421; fax: +1 302 831 3619.
E-mail address: santare@udel.edu (M.H. Santare).

0378-7753/$ – see front matter © 2011 Elsevier B.V. All rights reserved.
doi:10.1016/j.jpowsour.2011.01.028

However, little work has been published on the effect of fuel cell geometry on the membrane stresses. Thus, we investigate the effect of cell width and land–groove width ratio as well as the effect of gas channel alignment on membrane stress through numerical means. Additionally, we conduct a series of experimental compression tests to visualize and verify the effect of land–groove geometry.

In the following, we review the analytical formulation used to calculate the mechanical response of the membrane, followed by a summary of the numerical model. Then, the effects of GDL modulus and land–groove geometry on the membrane in-plane stresses will be studied and discussed.

2. Mechanics formulation

Here we outline the approach used to incorporate hygro-thermal effects into the finite element simulation. This is an extension of our previous work [8,10,12,22].

We assumed that the total strain tensor, ε_{ij} ($i, j = x, y, z$ or 1, 2, 3) can be written as the sum:

$$\varepsilon_{ij} = \varepsilon_{ij}^{\mathrm{el}} + \varepsilon_{ij}^{\mathrm{p1}} + \varepsilon_{ij}^{\mathrm{T}} + \varepsilon_{ij}^{\mathrm{S}} \tag{1}$$

where $\varepsilon_{ij}^{\mathrm{el}}$ is the elastic strain component, $\varepsilon_{ij}^{\mathrm{p1}}$ is the plastic strain component, and $\varepsilon_{ij}^{\mathrm{T}}$ and $\varepsilon_{ij}^{\mathrm{S}}$ are the temperature and swelling induced strains, respectively.

Thermal strain generated by the difference between the current temperature, T, and the reference temperature, T_0, is given by

$$\varepsilon_{ij}^{\mathrm{T}} = \alpha(T - T_0)\delta_{ij} \quad \text{with } \delta_{ij} = \begin{cases} 1 \text{ if } i = j \\ 0 \text{ if } i \neq j \end{cases} \tag{2}$$

where α is the linear coefficient of thermal expansion. The measured change in the volume of the membrane due to water uptake was used to derive the swelling strain, through the introduction of an anisotropy ratio of swelling, ξ_i, which satisfies the condition $\xi_x + \xi_y + \xi_z = 1$. Specifically,

$$\varepsilon_{ij}^{\mathrm{S}}(i) = \delta_{ij}\xi_i \ln\frac{V}{V_0} = -\delta_{ij}\xi_i \ln\phi_{\mathrm{p}} \tag{3}$$

where V and V_0 are the final (swollen) and initial (dry) volume of the polymer membrane, respectively, and $\phi = V_0/V$ is the polymer volume fraction ($\phi_{\mathrm{p}} = 1 - \phi_{\mathrm{w}}$).

In the reinforced membranes considered in this study, a ten-fold increase in swelling strain was assumed in the out-of-plane direction compared to the in-plane direction [23], corresponding to anisotropy ratios of $\xi_x = \xi_z = 1/12$ and $\xi_y = 10/12$. In this case,

$$\begin{aligned} \varepsilon_{ij}^{\mathrm{S}}(x) &= \varepsilon_{ij}^{\mathrm{S}}(z) = -\frac{1}{12}\delta_{ij} \ln(1 - \phi_{\mathrm{w}}) \\ \varepsilon_{ij}^{\mathrm{S}}(y) &= -\frac{10}{12}\delta_{ij} \ln(1 - \phi_{\mathrm{w}}) \end{aligned} \tag{4}$$

In order to account for the effect of temperature, we introduced a temperature dependent relationship:

$$\varepsilon_{ij}^{\mathrm{S}}(i) = -\delta_{ij}\xi_i \frac{T}{T_0} \ln(1 - \phi_w) \tag{5}$$

By definition, the water volume fraction can be determined from the water content:

$$\phi_{\mathrm{w}} = \frac{18\lambda}{(\mathrm{EW}/\rho_{\mathrm{p}}) + 18\lambda} \tag{6}$$

where the water content, λ, is the number of water molecules attached to each sulfonic acid SO_3^- group, EW is the equivalent weight and ρ_{p} is the density of dry polymer membrane. The parameter λ quantifies the hydration state of a perfluorosulfonic acid membrane, the reference material used in most PEMFCs. In this study, water content ranges from 2 to 14, corresponding to the hydration in equilibrium with air at relative humidity from 30% to 100%. We determined the water content in the PFSA membrane from an empirical formula, which gives similar water content numbers to relationships found in the literature [24,25]. The reference state was assumed to be $T_0 = 25\,^\circ$C, at which $\varepsilon_{ij}^{\mathrm{T}} = \varepsilon_{ij}^{\mathrm{S}} = 0$.

The constitutive response of the MEA in the elastic region was given by the linear Hooke's law, for which the stress tensor:

$$\sigma_{ij} = \frac{E}{(1+\nu)(1-2\nu)}[\nu\varepsilon_V^{\mathrm{el}} + (1-2\nu)\varepsilon_{ij}^{\mathrm{el}}] \tag{7}$$

where $\varepsilon_{ij}^{\mathrm{el}} = \varepsilon_{xx} + \varepsilon_{yy} + \varepsilon_{zz}$, ν is Poisson's ratio, δ_{ij} is the Kronecker delta defined previously, and E is the Young's modulus.

To characterize the plastic constitutive response in the plastic region, we adopted the Mises yield criterion (J_2-flow theory) [26]:

$$f(\sigma_{ij}, \bar{\varepsilon}^{\mathrm{pl}}) = \sqrt{\frac{3}{2}S_{ij}S_{ij}} - \sigma^{\mathrm{Y}}(\bar{\varepsilon}^{\mathrm{pl}}, \phi_{\mathrm{w}}, T) \tag{8}$$

where $\bar{\varepsilon}^{\mathrm{pl}}$ is the current equivalent plastic strain, σ^{Y} is the yield strength and S_{ij} are the components of the deviatoric stress tensor defined by

$$S_{ij} = \sigma_{ij} - \frac{1}{3}(\sigma_{xx} + \sigma_{yy} + \sigma_{zz})\delta_{ij} \tag{9}$$

where σ_{ij} are the components of the true stress tensor. The material exhibits plastic deformation when the flow function $f > 0$. In this work, the yield stress of the material was defined as a function of water volume fraction, temperature and equivalent plastic strain, $\bar{\varepsilon}^{\mathrm{pl}}$, which is a measure of the accumulated plastic strain during inelastic (permanent) deformation. As the equivalent plastic strain increases, we assume that the yield surface expands so that the material exhibits isotropic hardening behavior.

3. Numerical model

3.1. Assumptions

A 2-D numerical model depicted in Fig. 1 was developed based on the following assumptions.

1) The components were assumed to be perfectly bonded along their interfaces (a parametric study investigating the interface conditions between the layers showed that an interfacial frictional contact results in similar response as the bonded condition).
2) A series of equilibrium states were simulated.
3) Temperature and water content throughout the membrane and electrodes (MEA) were assumed to be uniform.
4) The material properties and the diffusion coefficient for the membrane and the electrodes were incorporated into the model as functions of temperature and water content.
5) The material response of the membrane and the electrodes was assumed to be time-independent (justifications for this assumption are (a) a complete set of visco-elastic-plastic properties, as functions of temperature and humidity, does not yet exist; (b) the time-independent simulations correspond to the limiting case of "rapid cycling"; and (c) our preliminary time-dependent results show that this "rapid cycling" produces higher maximum stresses in the membrane than the time-dependent response and therefore represents a sort of "worst case").
6) For the GDL and the bipolar plates, the deformation was assumed linear–elastic with no swelling, whereas the membrane and electrodes were allowed to deform plastically with isotropic hardening and anisotropic swelling.
7) The remaining material properties of the bipolar plates and MEA were isotropic.

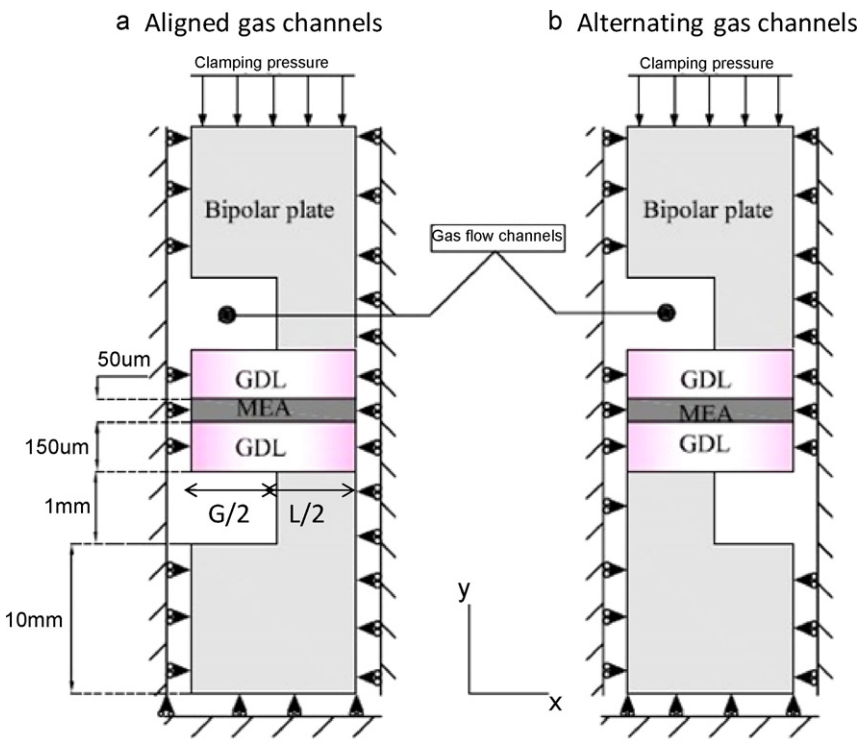

Fig. 1. The two geometries modeled, where the flow field has either (a) aligned or (b) alternating gas channels. The mechanical boundary conditions are noted in the figure. Constant pressure clamping is applied at the top of upper bipolar plate.

8) The properties of the GDL were investigated via a parametric study.

3.2. Geometry and boundary conditions

We have constructed a two-dimensional finite element model containing bipolar plates, gas diffusion layers (GDLs), electrodes and a proton exchange membrane (PEM) for use in the commercial software ABAQUS 6.7 (Fig. 1). Utilizing symmetry, only half of a unit cell was modeled. This model is an adaptation and extension of our previous work [8,10,12,22]. Two gas channel alignments were studied: *aligned* and *alternating*, and the cell layers thickness dimensions are depicted in Fig. 1. Gas flow channel and land widths are not indicated explicitly as they were varied in this study as discussed below.

Zero displacement boundary conditions were applied at the bottom and two sides of the unit cell. In our previous models, periodic conditions were applied to the sides, but we found that, due to the high stiffness of the bipolar plates, the zero displacement condition gives essentially the same results. A constant clamping pressure of 1 MPa was applied on the surface of upper bipolar plate throughout the simulations. The coordinates were chosen such that the in-plane and the out-of-plane (through-the-thickness) directions coincide with the x- and y-axis, respectively. It was presumed that the depth of the cell (in the z-direction) is much larger than its width and thickness, so that generalized plain strain conditions were assumed in the model (strain in the z-direction constant).

Eight node, reduced integration coupled-temperature displacement generalized plane strain hybrid elements (CPEG8RHT) were used for the simulations. A mesh study was performed in order to ensure the mesh was adequately refined and it was determined that around 6000 elements with 30,000 nodes were adequate for a typical model.

3.3. Material properties

The bipolar plates, whether metal or graphite, are many times stiffer than other cell components. Consequently, their specific mechanical properties do not significantly affect the membrane stresses. In this study, the material properties for the bipolar plates were set to those of commercial graphite for consistency, with Young's modulus of 10 GPa and Poisson's ratio of 0.49. For the GDL, the properties of a commercial carbon paper provided by SGL were used [27]. Our preliminary in-plane tensile tests for the SGL commercial carbon paper indicated a linear–elastic behavior for the strain range of interest here, with Young's modulus independent of temperature and humidity. Additional tests of the elastic properties of SGL commercial carbon paper have independently been conducted at SGL, Nuvera and the University of Delaware. The results showed that the elastic properties through the thickness are significantly different than the in-plane properties. Specifically, the modulus in the thickness direction is more than two orders of magnitude lower than the in-plane modulus. Furthermore, Kleemann et al. [28] found that the anisotropic Poisson's ratios for the GDL are nearly zero. Based on these different sets of measurements, we assumed the following base properties for the GDL: $E_x = E_z = 1500$ MPa, $E_y = 9$ MPa, $\nu_{xy} = \nu_{xz} = \nu_{yz} = 0$. We also studied a range of different GDL properties to investigate their effect on the membrane stresses. In all cases, we assumed that the GDL has linear–elastic behavior and does not swell in response to moisture.

For the membrane, the mechanical properties were determined previously from tensile tests at sixteen temperature humidity combinations, of an experimental reinforced membrane provided by W.L. Gore & Associates [23]. The electrode properties were obtained as functions of temperature and water content in a similar fashion to the membrane. These properties were incorporated into the numerical model. Details pertaining how the tests were conducted

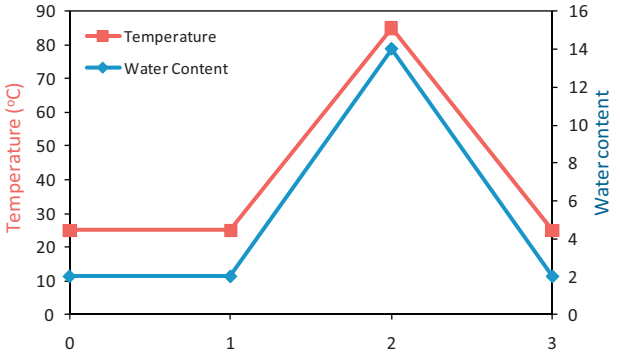

Fig. 2. Hygro-thermal loading/unloading cycle.

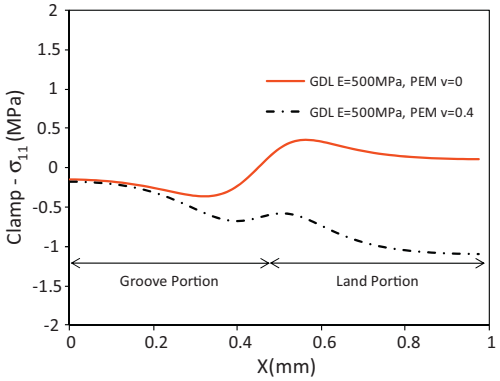

Fig. 4. In-plane stress as a function of horizontal position at the mid-plane of the membrane after clamping.

and the experimental data incorporated into the numerical model can be found in our previous paper [22].

3.4. Simulation of a hygro-thermal loading/unloading cycle

The hygro-thermal cycle was simulated by first defining a set of initial conditions followed by the imposition of three (ABAQUS) load steps, as shown in Fig. 2.

The initial conditions correspond to a zero stress-state at ambient temperature and water content, 25 °C and $\lambda = 2$, respectively.

Step 1: Clamping: a fixed pressure of 1 MPa is imposed and held constant throughout the rest of the simulation.
Step 2: Hydration: hygro-thermal loading is applied by linearly increasing the water content and temperature of the MEA up to $\lambda = 14$ and 85 °C.
Step 3: Dehydration: hygro-thermal unloading is achieved by linearly decreasing the water content and temperature to the initial values.

During the cycle, the water content and temperature are assumed to be uniform over the MEA. This simplified cycle corresponds roughly to taking the cell from ambient conditions, through start-up, to a hydrated condition and then back to shut-down, assuming the cell is allowed to dryout during shut-down.

4. Results and discussion

4.1. Effect of GDL modulus on stresses in the membrane after clamping

To investigate how GDL modulus affects the membrane in-plane stresses (σ_{11}) after clamping, we conducted a series of parametric studies using the aligned gas channel geometry with $L = G = 1000$ μm, where L and G are defined in Fig. 1.

To simplify the problem initially, we started by considering isotropic GDL properties. Three different GDL moduli (9 MPa, 500 MPa and 3000 MPa) were used. Furthermore, the interactions between the deformation of the GDL and the membrane can result in a complex state of stress. Therefore, in order to separate the lateral deformation of the GDL from that of the membrane, a Poisson's ratio of 0 was assumed for the membrane. As shown in Fig. 3, we found that a through-the-thickness gradient in the horizontal deformation occurs in the GDL (a bending-like rotational deformation), resulting in a negative in-plane stress (compression) in the membrane under the groove portion of the bipolar plate and a positive in-plane stress (tension) under the land portion. Fig. 3b also shows that when the GDL modulus is large, the in-plane stress in the membrane becomes small as this bending-like deformation gradient effect becomes less significant.

When Poisson's ratio of 0.4 (the actual value) is used for the membrane, the membrane stress distribution clearly combines the "Poisson's effect" and the "GDL deformation effect". The in-plane stress becomes more negative (more compressive) along the entire width of the model, Fig. 4. This is because the Poisson's effect, from the applied vertical compression, adds an overall compressive in-plane stress to the membrane. Furthermore, the membrane under the land portion compresses more than under the groove portion since the vertical pressure on the land portion is larger. By studying the deformation under these different conditions, we can see that the in-plane stress in the membrane after clamping is due to two factors: the effect from the through-the-thickness deformation gradient in the GDL, and the effect from Poisson's ratio of the membrane.

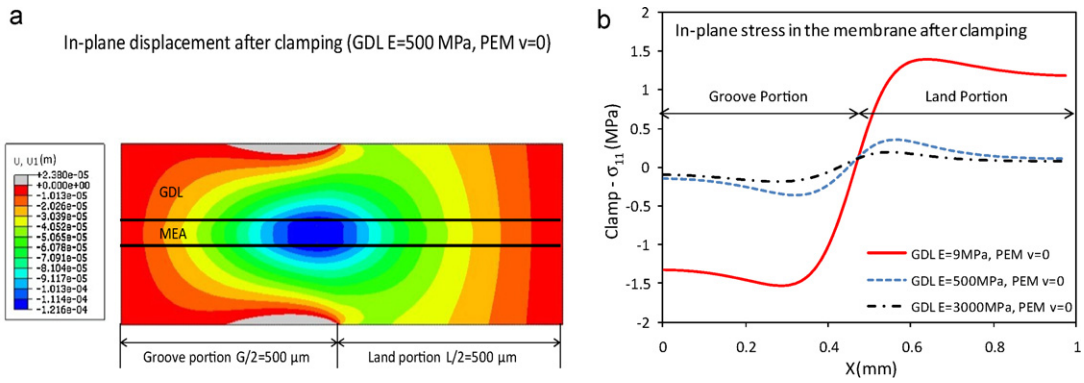

Fig. 3. (a) In-plane displacement and (b) in-plane stress as a function of horizontal displacement at the mid-plane of the membrane after clamping due to bending-like deformation in GDL ($\nu = 0$). $L = G = 1000$ μm.

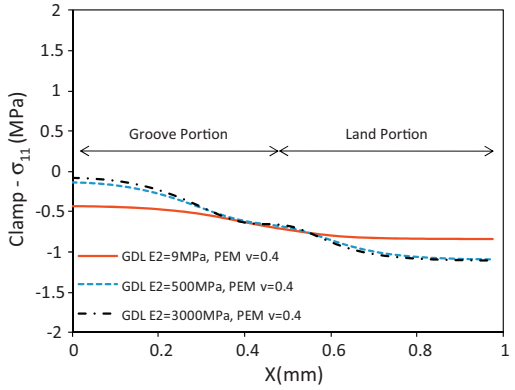

Fig. 5. In-plane stress as a function of horizontal position after clamping when anisotropic moduli are used in the GDL.

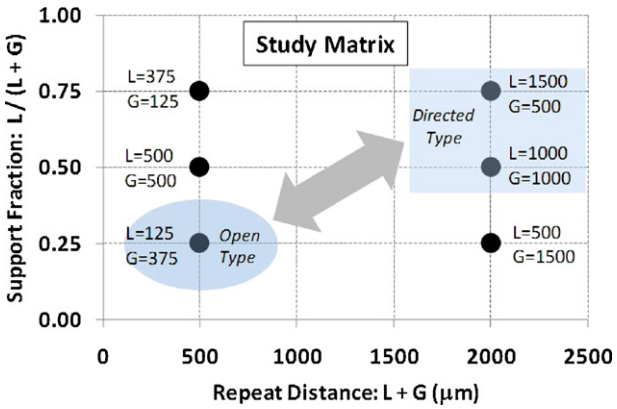

Fig. 6. Study matrix of repeat distances and support fraction values (i.e. groove and land widths) investigated (L and G are defined in Fig. 1).

Following this initial study using isotropic GDL properties, we next introduced anisotropic GDL properties. The modulus of the GDL in both in-plane directions was fixed at 1500 MPa and we investigated three through-the-thickness moduli (9 MPa, 500 MPa and 3000 MPa), all with the membrane Poisson's ratio of 0.4. As shown in Fig. 5, we found that for the anisotropic GDL, varying the through-the-thickness modulus of the GDL has a small effect on the in-plane stress in the membrane after clamping. Since the GDL is relatively stiff in the in-plane direction, the GDL bending-like deformation effect is relatively small and the in-plane stress in the membrane is dominated by the membrane Poisson's effect.

4.2. Effect of land–groove geometry on stresses in the membrane

In this section, the effects of (unit) cell width and land–groove width ratio as well as gas channel alignment on the membrane in-plane stresses are discussed. For all cases shown here, the GDL has the following anisotropic elastic properties: $E_x = E_z = 1500$ MPa, $E_y = 9$ MPa, $\nu_{xy} = \nu_{xz} = \nu_{yz} = 0$. For the membrane, Poisson's ratio is kept at 0.4.

4.2.1. Effect of cell width and land–groove width ratio

The ranges of values for the cell width and land–groove width ratio are based on state-of-the-art flow fields, and include cases representative of both directed and open flow field types. The study matrix is illustrated in Fig. 6.

For aligned gas channels as shown in Fig. 1a, we first fixed the land–groove width ratio at $L/(L+G) = 0.50$, and compared the stresses at the mid-line of the membrane for a wide cell $L+G = 2000$ μm and a narrow cell $L+G = 500$ μm. L and G correspond to the width of the bipolar land (rib) and groove (gas flow channel), respectively, and $L+G$ is the total unit cell. Fig. 7 shows that the variation in stress (difference between maximum and minimum) in the narrow cell case is smaller than in the wide cell case. This is because the clamping force is distributed more evenly in the narrow cell case. However, the two cases have the same average stresses as required by the fixed pressure loading condition.

Secondly, we chose a fixed cell width $L+G = 2000$ μm, and compared the stresses when the land–groove width ratio, $L/(L+G)$ varies. From Fig. 8 we see that in all cases, the average stress is constant. Moreover, larger $L/(L+G)$ ratio results in smaller stress variation. The results suggest that, with the other dimensions unchanged, narrowing the cell width or increasing the land–groove

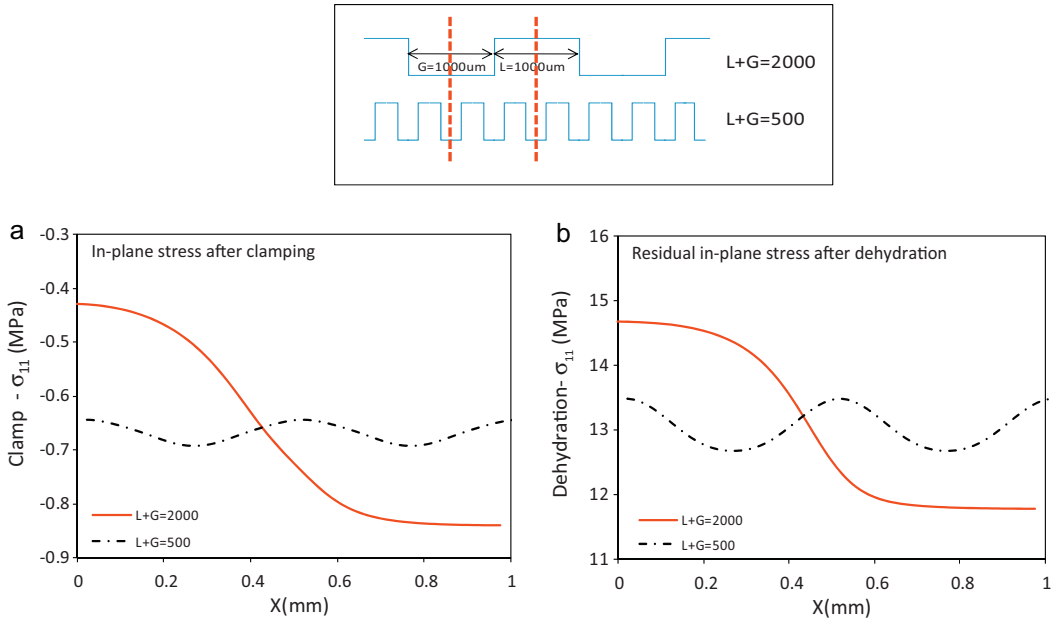

Fig. 7. (a) In-plane stress after clamping and (b) residual in-plane stress after dehydration as a function of horizontal position at the mid-plane of the membrane when $L/(L+G) = 0.50$. The narrow cell case is plotted four times in order to compare with the wide land case on the same horizontal axis.

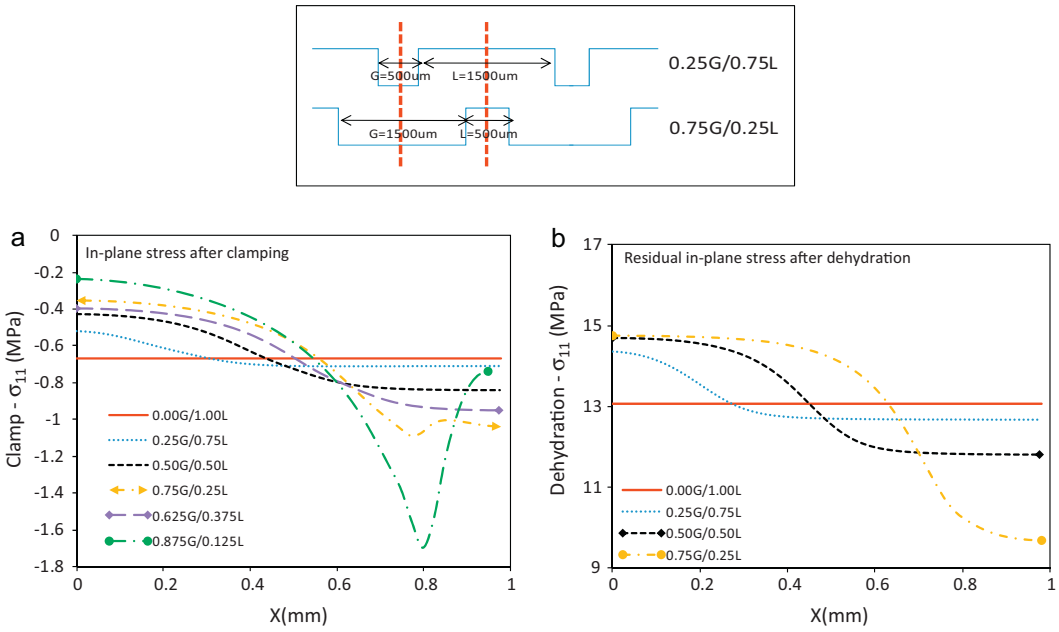

Fig. 8. (a) In-plane stress after clamping and (b) residual in-plane stress after dehydration as a function of horizontal position at the mid-plane of the membrane when $L+G=2000$ μm.

width ratio $L/(L+G)$ can give more uniform membrane stresses. From Fig. 8a we also see that the narrow land cases ($0.75G/0.25L$ and $0.875G/0.125L$) show a spike in the compressive stress around the land edge. We believe that this is because when the land width is large compared to the MEA–GDL thickness, the bipolar land causes a bending deformation in the MEA–GDL. However, when the land width approaches the MEA–GDL thickness, the bipolar land acts more like a rigid indenter, causing a stress concentration under the edge of the land.

4.2.2. *Effect of gas channel alignment*

In general, the gas channels on either side of the GDL may not be aligned with each other. Therefore, in addition to the aligned gas channels, alternating gas channels, as shown in Fig. 1b, were also studied. Comparison of the stresses at the mid-line of the membrane for a wide cell $L+G=2000$ μm and a narrow cell $L+G=500$ μm for the land–groove width ratio at $L/(L+G)=0.50$ is shown in Fig. 9. For the alternating cases, it is found that a wide cell produces tensile in-plane stress after clamping, due to stretching of the membrane in the in-plane direction as shown in Fig. 10b. Additionally, we see that the wide cell case produces larger residual in-plane stress than the narrow cell case. We also found that for the alternating cases, the narrow cell results in similar in-plane stress magnitudes to the aligned cases, but produces a more uniform stress distribution.

In Fig. 11, we fixed the cell width at $L+G=2000$ μm, and compared the stresses at the mid-line of the membrane for different land–groove width ratios in the aligned and alternating gas channel geometries. For the alternating cases, the in-plane stress after clamping increases from a compressive value to a tensile value as the land–groove width ratio decreases. Moreover, reducing the land–groove width ratio increases the residual in-plane stress. This increase becomes especially significant in the narrow land case ($0.75G/0.25L$). It needs to be pointed out that the lands do not overlap in this case. When the land–groove width ratio becomes large (for example, $L/(L+G)=0.75$), the two alignments produce similar in-plane stress magnitudes as the land overlap increases and thus the effect of channel alternation diminishes. For the alternating cases, the location of the maximum residual in-plane stress changes from the two ends of the solution domain for the large land–groove ratios to the middle as the land–groove width ratio decreases. The maximum residual stress is always at the

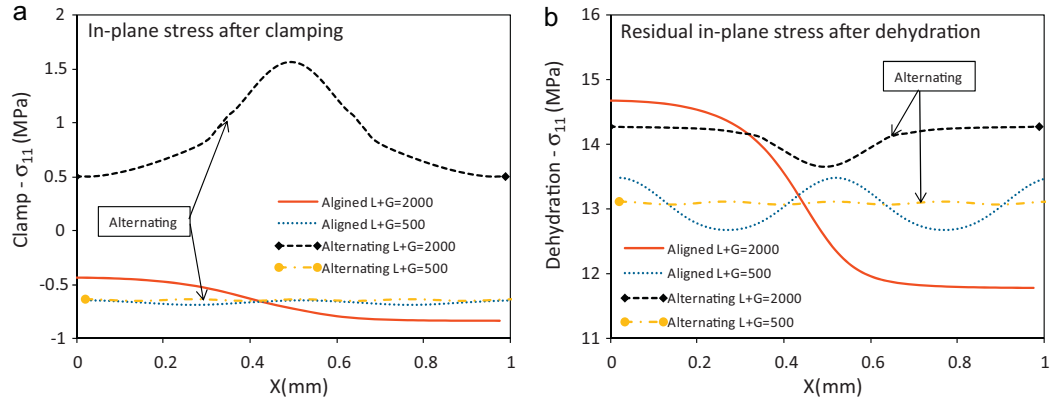

Fig. 9. (a) In-plane stress after clamping and (b) residual in-plane stress after dehydration as a function of horizontal position at the mid-plane of the membrane for the two alignments when $L/(L+G)=0.5$ and $(L+G)$ is varied.

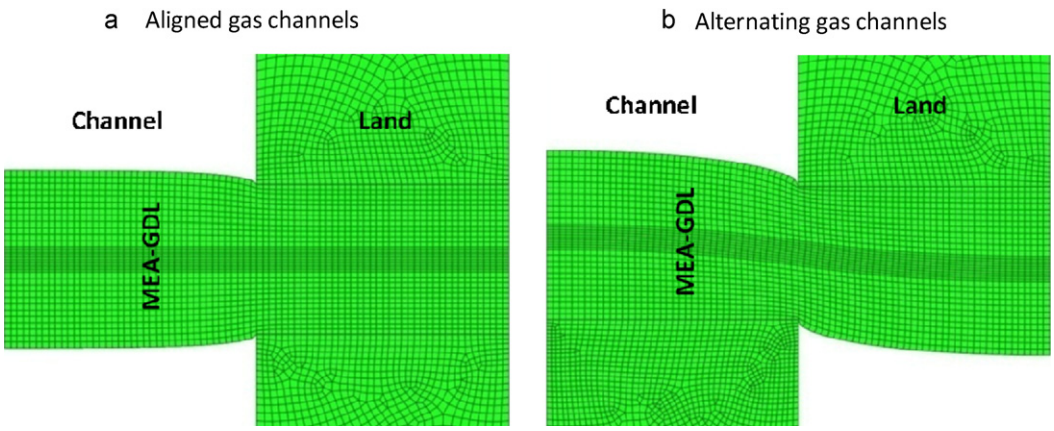

Fig. 10. Deformation of the model after clamping: (a) aligned gas channels and (b) alternating gas channels. $L+G=2000$ μm and $L/(L+G)=0.50$.

left end of the domain (middle of the groove) for the aligned cases.

In summary, when the gas channels are aligned, the cell width and land–groove width ratio affect the membrane stress distribution but do not significantly affect the overall stress magnitudes. However, when the gas channels are alternating, the cell width and land–groove width ratio significantly affect the stress magnitudes. Furthermore, when the cell width is small or the land–groove ratio is large, the two alignments produce similar in-plane stress magnitudes. Figs. 7–9 and 11 also show that tensile residual stresses in the membrane after hygro-thermal unloading are much higher than the stresses after clamping. These high stresses may explain the appearance of cracks and pinholes in the membrane under cyclic loading [8].

4.2.3. *Experimental compression tests to verify the effect of land–groove geometry*

In addition to the numerical work, a series of experimental compression tests on test cell units were conducted using an Instron™ machine, producing photographic images corresponding to the clamping step simulated in the numerical model. The intent was to have qualitative confirmation of the numerical results. The width of the experimental models assembled had a repeat unit cell width of $L+G=2000$ μm. The applied load was 1 MPa, accounting the entire area of the electrochemical area. The nominal case had $L/(L+G)=0.5$, and replicates one of the simulated cases identically. To more dramatically illustrate the deformations, more extreme values of the $L/(L+G)$ ratio were selected, viz. 0.125 and 0.875, which exceeded the simulated cases of 0.25 and 0.75. In all cases, aligned and alternating gas channel geometries were contrasted.

To properly compare the simulation results and the visualizations, it is important to note a major distinction. In the cells shown in the photographs, the flow field plates have finite width and are mechanically constrained at their lateral ends. The simulated geometries were generated using a periodic boundary condition so they simulate an infinite lateral dimension. Thus, the deformations and stress levels predicted by the simulations will be over predicted for an actual hardware assembly.

From Fig. 12, we found that when the gas channels are aligned or the gas channels are alternating with a large land–groove width ratio (for example, $L/(L+G)=0.875$), the membrane is compressed uniformly in the compression test. However, when the gas channels are alternating and the land–groove width ratio is small (for example, $L/(L+G)=0.50$ and 0.125), non-uniform deformation in the through-the-thickness direction causes stretching of the membrane in the in-plane direction. The deformation in the test cells is similar to the numerical results.

The photos also reveal some interesting physical phenomena not able to be predicted by the numerical model. Specifically, they show that the fiber structure of the GDL is to some extent damaged during the compression test, as evidenced by fiber strands that are observed in the channel space away from the GDL proper. The photos also show that the fiber structure of the GDL is damaged more for the alternating cases, and that the smaller the land–groove width ratio $L/(L+G)$, the more severe the damage. The deformation seen in the photos also suggests that the GDL transfers compression pressure from the land area to the channel area.

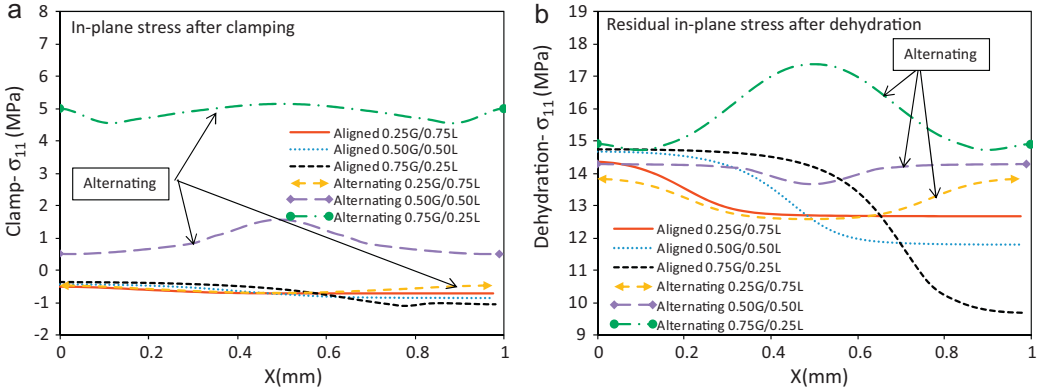

Fig. 11. (a) In-plane stress after clamping and (b) residual in-plane stress after dehydration as a function of horizontal position at the mid-plane of the membrane for the two alignments when $L+G=2000$ μm and $L/(L+G)$ is varied.

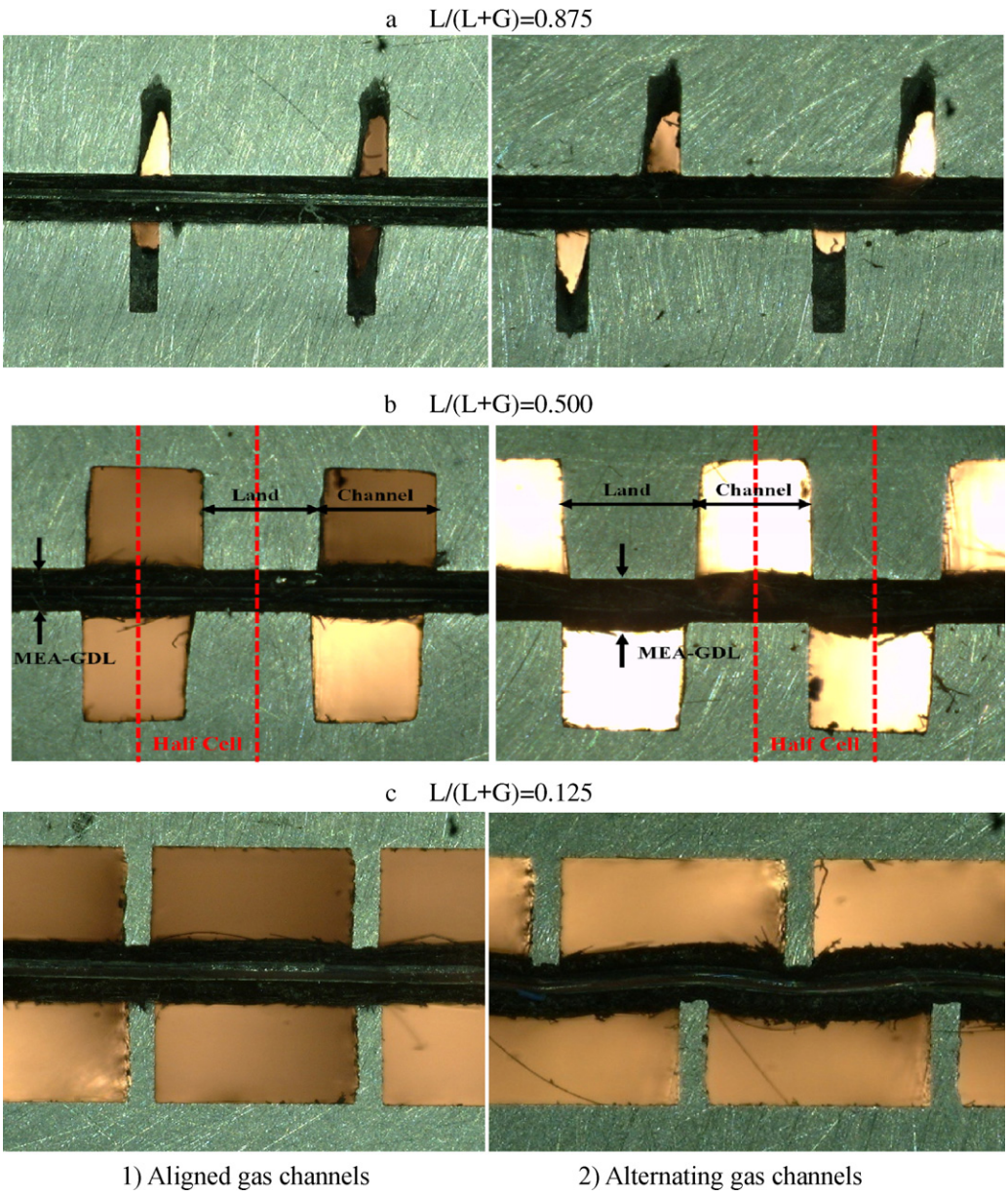

Fig. 12. Photos of test cell units with selected land–groove geometry after compression tests (corresponding to the clamping step in the numerical model). The total width of a unit cell is chosen as $L+G=2000$ μm.

5. Concluding remarks

In the aligned gas channel geometry, the effect of the GDL modulus on the in-plane stress in the membrane after clamping has been investigated. The parametric study included both isotropic and anisotropic GDL properties. From the results with isotropic GDL properties, we found that the in-plane stress in the membrane after clamping is due to two factors: the effect from the through-the-thickness deformation gradient (bending-like rotational deformation) in the GDL and the Poisson's effect in the membrane. The GDL bending produces compression on the groove portion of the membrane, and tension on the land portion. However, the Poisson's effect from the membrane produces in-plane compression everywhere in the membrane. We also found that increasing the GDL modulus results in a decrease in the GDL bending effect. For the anisotropic GDL properties, however, varying the through-the-thickness modulus of the GDL does not significantly affect the in-plane stress in the membrane after clamping.

Furthermore, we also investigated the effect of cell width and land–groove width ratio as well as gas channel alignment on the membrane in-plane stresses during a simplified hygro-thermal cycle. We found that for aligned gas channel geometries, the cell width and land–groove width ratio affect the stress distribution. Specifically, smaller cell width and larger land–groove width ratios result in more uniform stresses in the membrane. However, the cell width and land–groove width ratios do not significantly affect the stress magnitudes, and the maximum residual in-plane stress in the membrane always occurs at the left end of the solution domain (middle of the groove). For alternating gas channel geometries, the cell width and land–groove width ratio were found to have significant effect on the membrane in-plane stress magnitudes. We found that for the alternating cases, the wide cell case can produce tensile in-plane stress after clamping due to stretching of the membrane. Also, for the alternating geometries, the wide cell cases produce larger residual in-plane stress than the narrow cell cases. We also found that for the alternating cases, the in-plane stress after clamp-

ing increases from a compressive value to a tensile value as the land–groove ratio decreases. Reducing the land–groove width ratio increases the residual in-plane stress significantly and changes the location of maximum residual in-plane stress from the two ends to the middle of the unit cell. In addition, when the cell width is small or the land–groove ratio is large, the two alignments produce similar in-plane stress magnitudes.

In addition to the numerical work, a series of experimental compression tests, which correspond to the clamping step in the numerical model, were conducted to visualize and verify the effect of land–groove geometry. While the assembled cells have a mechanical constraint that restricts displacement and the corresponding stresses, unlike the simulated cases, the deformation in the real unit cells is similar to the numerical results. Lateral transfer of the compression pressure through the GDL was also observed.

Acknowledgement

This research has been supported by Nuvera under a grant (DE-FG36-07GO17014) from the United States Department of Energy. The commercial carbon paper and reinforced membrane used in this study were provided by SGL and W.L. Gore, respectively.

References

[1] S. Cleghorn, J. Kolde, W. Liu, in: V. Wolf, L. Arnold, G. Hubert (Eds.), Handbook of Fuel Cells - Fundamentals, Technology and Applications, John Wiley & Sons, Ltd., 2003.
[2] M. Crum, W. Liu, ECS Transactions 3 (2006) 541–550.
[3] E. Endoh, S. Terazono, H. Widjaja, Y. Takimoto, Electrochemical and Solid State Letters 7 (2004) A209–A211.
[4] S. Kundu, M.W. Fowler, L.C. Simon, S. Grot, Journal of Power Sources 157 (2006) 650–656.
[5] W. Liu, K. Ruth, G. Rusch, Journal of New Materials for Electrochemical Systems 4 (2001) 227–231.
[6] V.A. Sethuraman, J.W. Weidner, A.T. Haug, L.V. Protsailo, Journal of the Electrochemical Society 155 (2008) B119–B124.
[7] Y.-H. Lai, C.S. Gittleman, C.K. Mittelsteadt, D.A. Dillard, Proceedings of the 3rd International Conference on Fuel Cell Science, Engineering, and Technology, Ypsilanti, MI, United States, 2005, pp. 161–167.
[8] A. Kusoglu, A.M. Karlsson, M.H. Santare, S. Cleghorn, W.B. Johnson, Journal of Power Sources 161 (2006) 987–996.
[9] M.F. Mathias, R. Makharia, H.A. Gasteiger, J.J. Conley, T.J. Fuller, C.J. Gittleman, S.S. Kocha, D.P. Miller, C.K. Mittelsteadt, T. Xie, S.G. Yan, P.T. Yu, Electrochemical Society Interface 14 (2005) 24–35.
[10] Y. Tang, M.H. Santare, A.M. Karlsson, S. Cleghorn, W.B. Johnson, Journal of Fuel Cell Science and Technology 3 (2006) 119–124.
[11] A.Z. Webber, J. Newman, AIChE Journal 50 (2004) 3215–3226.
[12] A. Kusoglu, A.M. Karlsson, M.H. Santare, S. Cleghorn, W.B. Johnson, Journal of Power Sources 170 (2007) 345–358.
[13] Y. Zhou, G. Lin, A.J. Shih, S.J. Hu, Journal of Power Sources 192 (2009) 544–551.
[14] W. Lee, C.H. Ho, J.W.V. Zee, M. Murthy, Journal of Power Sources 84 (1999) 45–51.
[15] J. Ge, A. Higier, H. Liu, Journal of Power Sources 159 (2006) 922–927.
[16] S. Escribano, J.F. Blachot, J. Etheve, A. Morin, R. Mosdale, Journal of Power Sources 156 (2006) 8–13.
[17] P. Zhou, C.W. Wu, Journal of Power Sources 170 (2007) 93–100.
[18] S. Shimpalee, J.W.V. Zee, International Journal of Hydrogen Energy 32 (2007) 842–856.
[19] J. Scholta, G. Escher, W. Zhang, L. Kuppers, L. Jorissen, W. Lehnert, Journal of Power Sources 155 (2006) 66–71.
[20] D.H. Ahmed, H.J. Sung, Journal of Power Sources 162 (2006) 327–339.
[21] S. Lee, H. Jeong, B. Ahn, T. Lim, Y. Son, International Journal of Hydrogen Energy 33 (2008) 5691–5696.
[22] A. Kusoglu, A.M. Karlsson, M.H. Santare, S. Cleghorn, W.B. Johnson, ECS Transactions 16 (2008) 551–561.
[23] Y. Tang, A. Kusoglu, A.M. Karlsson, M.H. Santare, S. Cleghorn, W.B. Johnson, Journal of Power Sources 175 (2008) 817–825.
[24] T.E. Springer, T.A. Zawodzinski, S. Gottesfeld, Journal of the Electrochemical Society 138 (1991) 2334–2342.
[25] T. Thampan, S. Malhotra, H. Tang, R. Datta, Journal of the Electrochemical Society 147 (2000) 3242–3250.
[26] R. Hill, The Mathematical Theory of Plasticity, Clarendon Press, Oxford, 1950.
[27] SGL, Product Information for Sigracet GDL, SGL Carbon Group.
[28] J. Kleemann, F. Finsterwalder, W. Tillmetz, Journal of Power Sources 190 (2009) 92–102.